Nuclear Instruments and Methods in Physics Research B 306 (2013) 49–53

Contents lists available at SciVerse ScienceDirect

Nuclear Instruments and Methods in Physics Research B

journal homepage: www.elsevier.com/locate/nimb

Hydrogen analysis and profiling with a position sensitive detector

M. Borysiuk [a,*], L. Ros [a], P. Kristiansson [a], H. Skogby [b], N. Abdel [a], M. Elfman [a], P. Golubev [a], E.J.C. Nilsson [a], J. Pallon [a]

[a] Division of Nuclear Physics, Department of Physics, Lund University, Box 118, SE-22100 Lund, Sweden
[b] Swedish Museum of Natural History, Department of Mineralogy, Stockholm, Sweden

ARTICLE INFO

Article history:
Received 24 July 2012
Received in revised form 11 December 2012
Accepted 12 December 2012
Available online 5 January 2013

Keywords:
Position sensitive detectors
Proton–proton scattering
Hydrogen analysis
Hydrogen depth profiling

ABSTRACT

The double sided silicon strip detector (DSSSD) is a segmented silicon detector commonly used in the fields of high energy physics and nuclear physics. This type of detector is used for analysis of reactions produced by charged particles. This makes it well suited for a number of analytical methods commonly used in ion beam analysis (IBA), such as Rutherford Backscattering (RBS) and elastic recoil detection (ERDA). One such detector was installed and tested at Lund Ion Beam Analysis Facility (LIBAF) recently. This is a modification to the existing setup used to measure hydrogen concentrations and depth profiles. When completed it will be used primarily for geological applications.

Exact knowledge of the hydrogen content is important in a number of fields, but high enough accuracy can be difficult to achieve with most methods. In IBA normally some variant of ERDA, such as the proton–proton (p–p) coincidence method is used. We describe how the p–p coincidence technique was optimized to get the most out of our experimental setup. Previously this type of spectroscopy has been performed with two detector channels. In the present setup we expand that number from 2 to 96 channels, 64 on the front and 32 on the back of the detector. The intersecting strips give 2048 distinct detector elements or 1024 possible coincidences as dictated by the reaction kinematics. This increase in complexity requires a more detailed data analysis but it rewards us with higher sensitivity and a better background suppression.

1. Introduction

Hydrogen is the most abundant element in the visible universe. It is capable of forming compounds with almost all other elements found in nature. It is also a common contaminant and since its presence affects a number of material properties, the study of hydrogen content and distribution is highly interesting and relevant for industrial applications [1,2]. The important fact for the present investigation is that hydrogen is a part of the most common and for us highly relevant molecule, namely water. Presence of water in earth's mantle is of great interest to geologists and is a subject of a large number of studies [2,3]. A variety of techniques have been used to measure hydrogen and compounds formed by hydrogen in geological samples. Fourier transform infrared spectroscopy (FTIR) and Raman spectroscopy are commonly used in this field, as is secondary ion mass spectroscopy (SIMS) [3]. The methods traditionally used by geologists for hydrogen measurement are relative methods, highly susceptible to matrix effects and so must rely on standards in order to provide quantitative results. On the other hand the absolute methods outside of IBA, such as thermogravimetric methods and hydrogen manometry require a large amount of material and high hydrogen concentrations [3–5].

Here, applied nuclear physics is uniquely positioned. In ion beam analysis (IBA), typically the only discernible effect of the sample matrix is that of the energy loss of the primary beam, or the reaction products in the sample. Geological samples are a thankful subject of study for a nuclear microprobe. They tend to be radiation resistant. Most of the techniques that fall under the umbrella of IBA are considered to be non-destructive, but MeV energy ions will cause radiation damage to samples, especially at large beam currents. The stability of geological samples means that often the only practical limitation is the time available for the sample analysis and the beam that a given facility can produce. IBA offers a few methods specific for hydrogen analysis. Several different nuclear reactions were extensively used in the past, especially $H(^{15}N, \gamma\alpha)^{12}C$ and $H(^{19}F, \gamma\alpha)^{16}O$, as were many variants of elastic recoil detection (ERDA). Those methods have been tested and used to study hydrogen concentrations as well as hydrogen profiles. They provide great depth resolution (<10 nm) but are limited to very thin layers. A review and a comparison of the most common IBA methods for hydrogen analysis can be found in [6–8].

* Corresponding author. Tel.: +46 462227733.
E-mail address: maciek.borysiuk@pixe.lth.se (M. Borysiuk).

0168-583X
http://dx.doi.org/10.1016/j.nimb.2012.12.040

2. Method

During the last decade, another approach to hydrogen analysis has been given more attention. Proton–proton scattering can be described as a variant of ERDA performed in transmission geometry in which both the scattered and recoiled particles are detected. This method has several advantages. It has been shown that irradiation damage to the sample is many orders of magnitude smaller for this method compared to the other commonly used IBA methods [9]. This is because damage to the sample scales as the Rutherford cross section while hydrogen detection scales with the non-Rutherford proton–proton scattering cross section. The technique is accessible with a simple setup, available at any IBA facility. It does not require heavy beams, like the above-mentioned NRA methods, or complicated detector system, like many variants of ERDA. The reaction cross section is high, enhanced by two orders of magnitude compared to the Rutherford cross section at the energy of few MeV available at most microprobe facilities [2]. Hence it is a perfect tool for microprobe analysis where often the low beam current is a limiting factor.

Proton–proton scattering was first proposed in 1972 by Cohen [10], who tested it with 17 MeV protons. The scattering cross section deviates significantly from the Rutherford cross section. It varies smoothly from 450 mb to 300 mb for angles of interest (which are 30°–60°) at the energy of 3 MeV. A high cross section allows the method to be combined with the low currents inherent to nuclear microprobe, in order to produce full three dimensional scans of thin samples [1,11] and measure hydrogen with concentrations of less than 0.1 ppm [12]. The only requirement for this method is that the samples need to be thin and preferably self-supporting. For the current study that means samples with a thickness on the order of 10 μm. This is why this method is perfectly suited for geological samples, since such samples can be polished to manageable size. In addition, interesting structures in geological samples are on the order of a few micrometers. This makes geological samples an interesting subject for a microprobe setup, which can produce a lateral resolution on the order of 1 μm.

Ultimately the power of the pp-scattering technique lies in its simplicity and specificity. In a simplest case this experiment should look as follows. A proton beam enters a thin target and interacts with a hydrogen atom found within. Both the beam proton and the recoiling hydrogen exit the sample with roughly half of the energy of the incoming proton (depending on the outgoing angle and the sample thickness). The kinematics of this elastic scattering process provides additional constraints beyond the coincidence condition between two particles. It is easy to show that the elastically scattered particles of equal mass will, in the lab coordinate frame, always scatter at an angle equal to 90°. In reality, the studied sample has a finite thickness, which adds the energy loss and straggling to the interaction and complicates the ideal picture. As mentioned before, this method has a high specificity, which generally means low background, and thus the theoretical limitation to the sensitivity comes primarily from the damage to the irradiated sample and loss of hydrogen from the material [9]. A simple way to improve the sensitivity of the method is to capture more coincidences per unit of charge the sample is subjected to, i.e. to increase the size of a detector as was done by [1]. This improvement comes at a price, as it also increases the number of accidental coincidences accepted. Additionally, a larger solid angle makes kinematics more complicated, especially for thick targets where multiple scattering becomes important. When the analyzed sample has a low hydrogen concentration the other limitation comes from the contribution from the hydrogen content on the surface of the sample. Since both particles involved in the reaction are detected, a complete reconstruction of the interaction is possible. The energy loss of the particles in the sample is a measure of the depth at which the interaction occurred. For a sample of known composition, the sum of the energies of the detected protons can be converted into depth profiles of the sample. When scattering occurs at or close to 45° angle relative to the incoming beam, which was an arrangement previously used in the pp-scattering method [2], the path of both the recoiled and scattered protons is equal and so the energy loss can be easily accounted for. For different scattering angles and thick targets additional angular information is helpful. The ability to discriminate the surface contamination from the bulk concentration is limited by the depth resolution of the setup. This in turn is limited by energy resolution and angular spread, which are a function of detector size, resolution and target thickness. The conclusion is that in order to take full advantage of the pp-scattering technique a new detector is required.

3. Experiment

The experiment described here was performed at the sub-micron beamline at the Lund Ion Beam Analysis Facility (LIBAF), which is discussed in detail in Ref. [13]. The facility consists of a single ended 3 MV Pelletron accelerator system designed and built by NEC, with three available ion beams: p, d and α. The typical beam spot diameter during this experiment was on the order of 20 μm with a beam current below 0.2 nA. The beam energy was close to the end of available range at 2.9 MeV. The vacuum in the target chamber during normal operation was below 1×10^{-5} mbar and below 5×10^{-6} mbar over the length of the entire accelerator vacuum system. This value is sufficient to provide good beam conditions, but it might be insufficient for the sample and result in excessive hydrogen contamination on the surface of the sample.

A position sensitive detector provides angular information and a large solid angle of detection. The currently tested detector is an annular 96 channel double sided silicon strip detector (DSSSD) similar to the one described in [14]. The highest sensitivity achieved to date with the pp-scattering technique was reached using a DSSSD, presented in [12]. The annular detector is a 500 μm thick single disc of silicon. It is divided into 64 sectors on the front face of the detector (they define granularity in the azimuthal angle φ) and 32 rings on the back (they define granularity in the polar angle θ). The total number of detector elements or pixels is $64 \times 32 = 2048$. Each pixel can be treated as a single detector in this scenario, which because of the kinematic restriction means that 1024 real coincidences can be detected in the optimal geometry. The outer active diameter is 85.4 mm while the inner active diameter is 32 mm. In the first approximation, it follows from the geometry of the detector and kinematic constraints of the reaction that the optimal detector sample distance to maximize the captured coincidence yield is around 26 mm. Assuming a point source and a disc shape detector with the dimensions given above an approximate active solid angle of the detector is 2 sr. Solid angle was calculated from the formula $\Omega = 2^{*}\pi^{*}(1 - \frac{d}{\sqrt{d^2+a^2}})$ which is an analytical solution of $\Omega = \int \frac{\cos(\alpha)}{r^2} dA$ for a disc detector. In the current experiment we are limited by mechanical constraints so that the actual detector sample distance was 21 mm, which means that used solid angle included only the first 12 rings or 1 sr. It is worth noting that in this configuration the size of a single pixel on the detector is around 1 msr. This high granularity gives good position sensitivity. Schematic picture of the detector setup is presented in Fig. 1.

Mesytec produced the analog electronics. Detector is read out with six 16-channel charge sensitive preamplifiers MPR-16. Four of them connected to the front side of detector, two to the back. The shaping amplifiers are the matching 16-channel STM-16

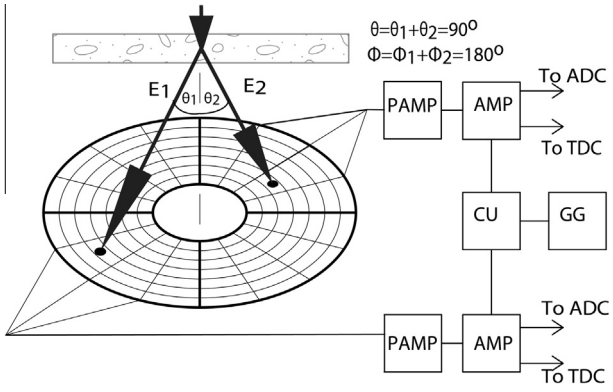

Fig. 1. This is a schematic description of the detector setup. Detector is an annular 96 strip DSSSD with 64 sectors on the front side and 32 rings on the back. Detector readout is divided into 6 sections, with 16 strips per section. This means that there are 4 quadrants (marked with thicker lines in the figure) on the front, covering 90° in the azimuthal angle each and 32 rings shaped strips on the back. The readout of rings is divided between even and odd rings. Each quadrant and both sets of rings are connected to its own electronics chain (preamplifier and amplifier). The amplifier produces shaped signals for the ADC, fast signals for the TDC and a trigger signal. The hardware trigger is a coincidence between the quadrants on the diagonal of the front face of the detector as illustrated in the figure. Two or more particles hitting the diagonal quadrants on the front face of the detector will be interpreted by hardware as a valid hit. Geometry of the detector is reconstructed in the software. This gives up to a total of 2048 pixels. Thanks to this reconstruction geometrical cuts can be placed on the data.

modules [15]. A hardware coincidence is created between the diagonal quadrants of the detector using standard NIM pulse electronic units with a coincidence time window of 200 ns. The charge measurement is preformed upstream from the target with an off-axis Faraday cup which is connected to a charge-to-frequency converter with sensitivity of 10 pA, as described previously in [16]. The beam is deflected into that cup once every 10 seconds for 1 second, in order to get a good average value of the current. Data acquisition was carried out using a VME based system that is still under development and is limited in capacity to 2000 gates/s. Analog signals were digitized using CAEN peak sensing ADCs v785 and CAEN v775 TDCs [17]. Data analysis as well as online monitoring was based on ROOT [18], which is an open source object oriented framework for data acquisition and analysis developed by CERN. This software gives us considerable freedom to create our own data analysis routine.

Calibration was performed using internal conversion electrons at 0.5 MeV and 1 MeV from a Bismuth-207 source and compared with the protons from the accelerator scattered off a 40 nm layer of gold at 2.9 MeV and alpha particles from a Thorium-232 source. Since both dead layer losses and non-ionizing contributions can be expected to be negligible for electrons with energy of 1 MeV [19], conversion electrons provide up to four discernible peaks that can be used for dead layer correction as well as energy calibration. In this way, the detector dead layer is estimated to be approximately 2 μm of Si equivalent material and the energy resolution is 20 keV at 1 MeV as measured with electrons.

The analysis of the actual hydrogen content in the samples can be performed without a standard, in which case the experimentalist relies on the detailed knowledge of the pp scattering cross section, in addition to the detailed knowledge of the detector geometry. To simplify matters in the analysis of the geological samples, an internal standard (Zoisite) with known stoichiometric hydrogen content and a chemical formula $Ca_2Al_3Si_3O_{12}(OH)$ will be used in the future. The notation preferred by geologist is water by weight since this is what FTIR is sensitive too and this is what is assumed to exist in the sample. However the pp-scattering method is sensitive to hydrogen only, which can be a source of some confusion. Both notations will be used for clarity. Zoisite has 1.98% of water by weight or 0.22% hydrogen by wt. and 4.54% at. of hydrogen. This mineral is often used as a standard in analysis of geological materials. This allows us to ignore most of the systematic errors except for the error in charge measurement.

4. Results

We performed the data analysis by placing successive cuts on the raw data collected and calibrated with our setup in a manner similar to the one presented in [8,9]. The specificity of the pp-scattering method defines a number of filters that can be applied to the raw data. We analyzed several samples, which are representative of the capacity of our setup. The geological samples are a 13 μm thick olivine $Mg_{1.6}Fe_{0.4}SiO_4$ with and a 10 μm thick garnet $Ca_3Fe_2Si_3O_{12}$. They have been previously analyzed and their hydrogen content was estimated to be 24 ppm by weight and 380 ppm respectively this corresponds to roughly 530 ppm at. and 0.76% at. of hydrogen [20]. A 15 μm Zoisite sample, which has high stoichiometric water content of 1.98% wt. or 4.54% of hydrogen at., is used throughout the rest of this section in order to exemplify the process of sample analysis.

The first restriction on the data is placed already in hardware and it takes the form of a coincident trigger between the opposite quadrants on the front surface of the detector with a window of 200 ns. This does not remove all accidental coincidences but it significantly reduces the flow of data to the disk and it means that in hardware this detector behaves as four large detectors in pair coincidence. The detector setup is shown schematically in Fig. 1. Due to the large angular size of the sectors a not insignificant portion of the background from accidental coincidences will remain, but that can be easily removed. In the first step we require the multiplicity of two particles and two particles only. The two spectra for the geological standard with and without the strict multiplicity condition are shown superimposed in Fig. 2. We show the intensity in arbitrary units as the function of the sum of the energies of the coincident particles, not the individual particle energies. The resulting spectrum consists of two broad peaks interfering with each other. The peak at lower energy in the spectrum corresponds to the true pp-coincidences. The peak at higher energy is caused by

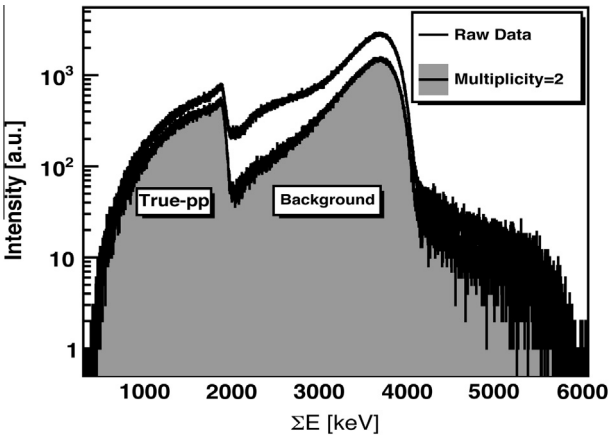

Fig. 2. This is the spectrum of the sum of energies of the two coincident particles. The peak at lower energy corresponds to proton–proton scattering. The peak at higher energy corresponds to elastic scattering of protons from heavier elements. Such energy sum plot after complete analysis can be used to extract the depth profiles and concentration in the sample, in this case mineral Zoisite with thickness of 15 μm. A simple multiplicity condition placed on the data results in a visible decrease in the elastic scattering background.

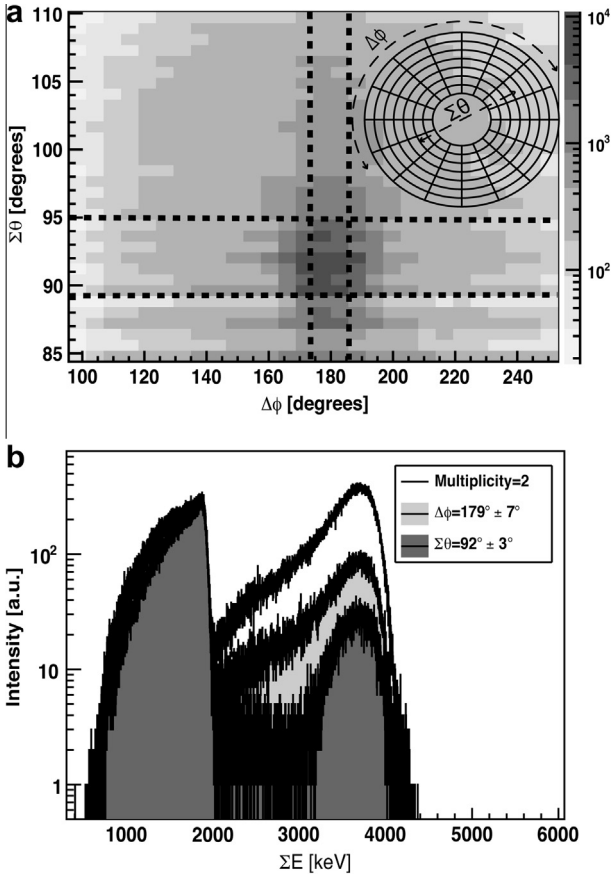

Fig. 3. (a and b). The kinematics of the reaction is such that real coincidences can be easily separated through purely geometrical considerations. A schematic image of the detector with the definition of the quantities plotted in (a) is presented in the inset in (a). The sum of polar angles of the two coincident particles $\Sigma\theta$, is plotted against the difference in their azimuthal angle $\Delta\Phi$. This results in a clear peak which we observe in a) at $\Delta\Phi = 179°$ and $\Sigma\theta = 92°$. The deviation from the expected value is most likely due to misalignment of the detector. The cut on that peak clears our spectrum considerably which can be seen in (b). We see that the two successive cuts remove large portion of accidental coincidences so that the signal to noise ratio increases by a factor of four. The analyzed sample is the geological standard Zoisite with a high water concentration of 1.98% that corresponds to hydrogen concentration of 4.54% at.

accidental coincidences that occur when two protons scatter from matrix atoms other than hydrogen. Alternatively this contribution could arise when a proton scatters from hydrogen, but only one true proton signal is detected and the other signal is supplied by a proton scattering from a matrix atom other than hydrogen. For a thin enough sample the two peaks will not interfere. In a thick sample with a heavy matrix the higher peak might provide a significant background and will affect the detection limit. This is the first condition set on the data and clearly more work is needed but the high background is indicative of high current on the sample. The high-energy edge of the lower (true-pp) peak corresponds to the pp scattering from the edge of the sample closest to the detector. The energy at this point is equal to the energy of the beam (2.9 MeV) minus the energy lost by the beam particle in the sample. This energy loss is a direct measure of the area density of the sample. For the current sample this edge is situated around 2 MeV, which means a sample thicker than 10 μm. The lower edge should correspond to the scattering from the other side of the sample and it means that one of the particles taking the longest possible path through the sample. Here it is assumed that no interfering reactions with large cross sections take place, which for a proton with of 3 MeV is a reasonable assumption.

It is worth noting that pixels shown in Fig. 1 are not physical structures on the detector. They are created in software when the frontside sectors are matched with backside rings for each valid event. The correct matching of front to back sectors allows us to recover the kinematic relation between the coincident particles and place further cuts on the data. From theory discussed earlier and in [8] we know that true pp coincidences will be separated by 90° in the polar angle and 180° in the azimuthal angle which for a correctly aligned detector means two pixels on opposite sides of the detector. This kinematic condition should result in a peak in a two dimensional spectrum where the angular distribution of the two particle events is plotted in a way that is indicated in the inset in Fig. 3a. This peak is indeed seen clearly in Fig. 3a. There is an error in the position of that peak. The peak is at 92° polar and 179° azimuthal, instead of 90° polar and 180°. Part of this error is due to the misalignment in the position of the detector relative to the beam from the calculated value. This gives an independent test of the geometry of the setup, which is an important factor in forward scattering experiment. The peak is also broad with FWHM = 3° in polar and FWHM = 7° in the azimuthal direction. This broadening is most likely due to multiple scattering. Both of these effects contribute to the smearing out of the peak in Fig 3a. We estimate that the observed error in angle corresponds to an error in position of <3 mm, since a larger error would shift the peak further. We make our pixels wider than one strip and shift the geometrical cut on the data from 90° to 92°. This should maximize the accepted true pp events. The proton energy sum spectra without and with the consecutive geometrical cuts applied can be seen in Fig. 3b. Once again the broad peak at lower energy corresponds to the true coincidences and the peak at higher energy is due to

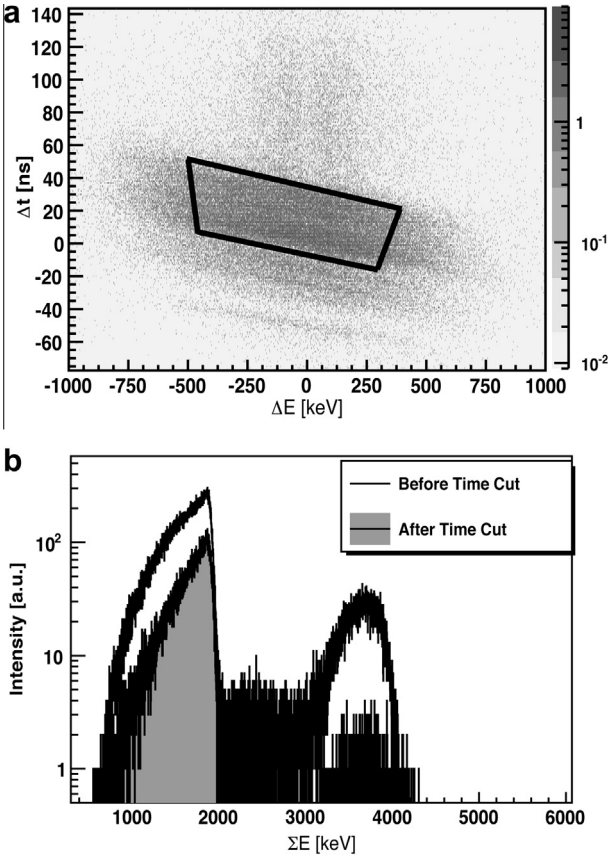

Fig. 4. a and b. The final step in the analysis is the cut on the Δt–ΔE plot for the two coincident particles. In (a) a band corresponding to the true coincidences can be seen and placing a 40 ns wide cut on this data removes most of the remaining accidental coincidences. This is shown in (b).

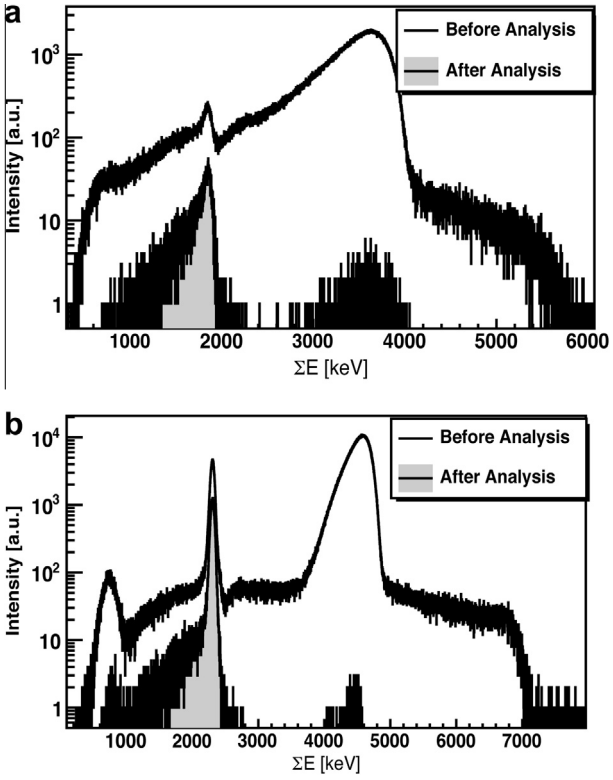

Fig. 5. a and b. Two cleaned up spectra for two different geological samples are presented in this figure. The sum of energies of the two incoming particles is plotted as in the Fig. 2. In (a) a Garnet with 380 ppm Hydrogen wt. or 0.76% at. and (b) olivine with 24 ppm wt. or 530 ppm at. In olivine hydrogen content on the surface of the sample is much higher then in the bulk. This hydrogen contamination on the surface of the olivine shows up as a clean peak and can be used to estimate the depth resolution which for this 13 μm thick sample is around 0.8 μm. The resolution will get worse deeper within the sample due to energy straggling. The background before the data analysis looks quite different for the two samples. As indicated in the body of the article the accidental coincidences come from proton scattering of the matrix atoms. Different matrix composition, account for the differences in background shape. Beauty of the coincidence method is that the data analysis removes almost all of the background leaving real pp-events, which can be converted to hydrogen concentration in the sample.

accidental coincidences. Since the sample is a thick one this peak will interfere with the true coincidences. After both geometrical cuts, the background near the pp peak decreased a factor of four and the signal to noise ratio (SNR) increased by a factor of four. The background can be easily seen by moving away from the 180° azimuthal separation. Here we will encounter multiply scattered particles and accidental coincidences only.

The final cut is the cut on the time difference for the two particles as the function of their energy difference. We see that cut and its results in Fig. 4a and b respectively. Real pp events are arranged in a band. It is expected that both Δt and ΔE will be nearly zero for particles scattering at 45° since in this case both particles should follow the same path. Both Δt and ΔE should increase for particles with different scattering angles like those coming at 30°/60°. This effect should be most pronounced in thick samples. The final result presented in Fig. 4b is an almost background free spectrum which can be used to estimate the hydrogen content relative to the standard sample.

In Fig. 5, the energy sum spectra from two actual geological samples are presented. All of the previously discussed cuts have been applied and the before and after histograms are superimposed. In both cases accidental coincidences decreased drastically. Estimated SNR increased 27 times in Fig. 5a so that SNR >20 with all the cuts applied. Since this sample has an estimated 530 ppm at. of hydrogen the current setup should be able to see down to some 20 ppm at. In Fig. 5b the content of hydrogen on the surface of the sample is much higher than in the bulk of the sample. We assume that this is a contamination limited to few atomic layers on the surface of the sample, and this gives us a sharp peak from which we estimate the achieved depth resolution near the surface of a thick geological sample to be 0.8 μm.

5. Conclusions

The goal of this experiment was to test the position sensitive detector as a tool for pp-scattering at LIBAF. As it was previously indicated [8], DSSSD is perfectly suited for this technique. Still a lot of work remains to be done. Mechanical difficulties when installing the detector in the target chamber means that suboptimal geometry was used and additionally the experiment suffered from the limitations in the DAQ capacity. This information will be used in future experiments to calculate the actual concentrations and depth profiles of hydrogen. Currently, the sensitivity lies around some tens of ppm. When fully functional the system should be able to reach sensitivity on the order of ppm in a reasonable time, for the samples of interest with a depth resolution better than 1 μm.

Acknowledgments

The support of the Swedish Research Council (VR) and Royal Physiographical society in Lund is acknowledged.

References

[1] K.A. Sjöland, P. Kristiansson, M. Elfman, K.G. Malmqvist, J. Pallon, R.J. Utui, C. Yang, Nucl. Instr. Meth. B 124 (1997) 639.
[2] M. Wegdén, P. Kristiansson, Z. Pastuovic, H. Skogby, V. Auzelyte, M. Elfman, K. Malmqvist, C. Nilsson, J. Pallon, A. Shariff, Nucl. Instr. Meth. B 219–220 (2004) 550–554.
[3] George.R. Rossman, Rev. Mineral. Geochem. 62 (2006) 1–28.
[4] Esther Schmädicke, Jürgen Gose, Patrick Reichart, Günther Dollinger, Am. Min. 93 (2008) 1613–1619.
[5] J.A. O'Leary, G.R. Rossman, J.M. Eiler, Am. Min. 92 (2007) 1900–1907.
[6] J.F. Ziegler et al., Nucl. Instr. Meth. 149 (1978) 19.
[7] W.A. Lanford, Nucl. Instr. Meth. B 66 (1992) 65.
[8] Y. Wang, M. Nastasi (Eds.), Handbook of Modern Ion Beam Materials Analysis, second ed., Materials Research Society, 2009.
[9] G. Dollinger, P. Reichart, G. Datzmann, A. Hauptner, H.-J. Körner, Nucl. Instr. Meth. B 197 (2002) 134.
[10] B.L. Cohen, C.L. Fink, J.H. Degnan, J. Appl. Phys. 43 (1972) 19.
[11] D. Dujmić, M. JakšiĆ, N. Soić, T. Tadić, I. Bogdanović, Nucl. Instr. Meth. B 111 (2006) 126–132.
[12] P. Reichart, G. Dollinger, A. Bergmaier, G. Datzmann, A. Hauptner, H.-J. Körner, R. Krücken, Nucl. Instr. Meth. B 219–220 (2004) 980–987.
[13] A. Shariff, C. Nilsson, V. Auzelyte, M. Elfman, P. Kristiansson, K. Malmqvist, J. Pallon, M. Wegdén, Nucl. Instr. Meth. B 231 (2005) 7–13.
[14] P. Golubev, P. Kristiansson, N. Arteaga-Marrero, M. Elfman, K. Malmqvist, E.J.C. Nilsson, C. Nilsson, J. Pallon, M. Wegden, Nucl. Instr. Meth. B 267 (2009) 2065–2068.
[15] http://www.mesytec.com/datasheets/MPR16.pdf (21.07.2012).
[16] P. Kristiansson, M. Borysiuk, N. Arteaga-Marrero, M. Elfman, E.J.C. Nilsson, C. Nilsson, J. Pallon, Nucl. Instr. Meth. B 268 (2010) 1727–1730.
[17] http://www.caen.it/csite/ProductList.jsp?parent=6&Type=Product (21.07.2012).
[18] R. Brun, F. Rademakers, Nucl. Instr. Meth. Phys. Res. A 389 (1997) 81–86.
[19] E. Steinbauer, P. Bauer, M. Geretschläger, G. Bortels, J.P. Biersack, P. Burger, Nucl. Instr. Meth. B 85 (1994) 642–649.
[20] J.L. Mosenfelder, M. Le Voyer, G.R. Rossman, Y. Guan, D.R. Bell, P.D. Asimow, J.M. Eiler, Am. Min. 96 (2011) 1725–1741.